MEASURING PHOTOMETRIC SURFACE ROUGHNESS WITH THE LUNAR ORBITER LASER ALTIMETER (LOLA). M. K. Barker[1], M. Karpenko[2], E. Mazarico[1], D. E. Smith[3], X. Sun[1], M. T. Zuber[3], T. P. McClanahan[1], G. A. Neumann[1], J. W. Head[4]. [1]Solar System Exploration Div., NASA Goddard Space Flight Center, 8800 Greenbelt Rd. Greenbelt, MD 20771 michael.k.barker@nasa.gov, [2]Dept. of Mechanical and Aerospace Engineering, Naval Postgraduate School, Monterey, CA 93943, [3]Dept. of Earth, Atmospheric & Planetary Sci., MIT, 77 Massachusetts Ave. Cambridge, MA 02139, [4]Dep. Earth, Env. & Planet. Sci., Brown Univ., Providence, RI, 02912.

Introduction: The Moon is a benchmark for understanding the effects of space weathering and geological processes on the surface properties of airless planetary bodies [1]. By studying the reflectance behavior of the lunar surface under different viewing and illumination conditions, we can learn about regolith properties such as grain size, shape, opacity, and the regolith surface textural properties like roughness and porosity [2]. The reflectance is measured as a function of the incidence, emission, and phase angles. Phase angles can be divided into two regimes: back-scatter at < 90°, and forward-scatter at > 90°. The LRO nadir pointing instruments are generally limited to phase angles < 120° due to solar keep-out zone constraints, but higher phase angles can provide more leverage on the forward-scattering phase function and surface roughness [3]. To that end, we are conducting a campaign with the Lunar Orbiter Laser Altimeter (LOLA) Laser Ranging (LR) telescope [4] to make photometric measurements at phase angles > 120°, a region of parameter space rarely probed by LRO. This campaign addresses key questions in lunar science related to regolith evolution and regolith photometric properties, such as *How does the small-scale structure of the lunar surface affect the photometric properties we observe? How do variations in the surface texture contribute to anomalous features, such as swirls and distal ejecta deposits? How, and how fast, are the albedo and texture of newly exposed materials altered? And, how does regolith development differ between different geologic settings?*

Instrument Description: For the high phase angle photometric observations discussed here, we are using LOLA as a passive radiometer to collect solar photons reflected off the lunar surface while the laser is turned off. These measurements are similar to the 1064-nm passive radiometry routinely collected by Channels 2 – 5 with the LOLA receiver telescope [5] except that, here, we are using Channel 1 with the LR telescope (LRT) at 532-nm [4], with a 1.75° field-of-view (FOV). Since it is mounted on, and co-boresighted with, the LRO high-gain antenna on the anti-nadir deck, the LRT is able to observe at much higher phase angles than the nadir-pointing instruments. The LRT is connected to the LOLA Channel 1 detector assembly (on the nadir deck) via fiber optic cable which feeds the signal through a narrow-band filter with central wavelength and band width of 532.25 ± 0.15 nm. The LRT can withstand direct solar illumination for up to ~2 hours, about the length of the LRO elliptical polar orbit. Pre-flight testing measured an off-axis transmission < 10^{-6} for angles > 10°. The exposure time and sampling rate is 0.0357 sec (28 Hz).

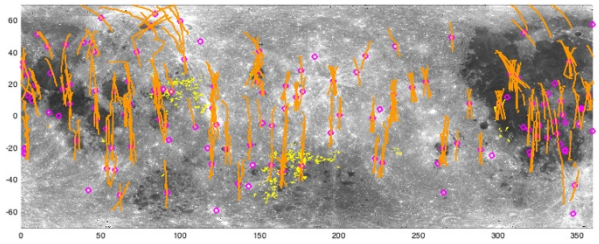

Figure 1 - Targets (pink circles), observed surface swaths (orange lines), and swirls (yellow; [7]) overlaid on a WAC 566-nm albedo basemap [8].

Preliminary Results: In a typical observation, LRO slews to point the HGA toward the horizon with the sun ~ 20 – 40° away. These slews are carefully designed to avoid occulting the star trackers of LRO's all-stellar attitude controller [6]. In 2019 and 2020, we executed 207 slews visiting 103 unique targets (Fig. 1), sampling a range of geologic settings such as Copernican-aged craters, the largest cold-spot craters, magnetic anomalies (swirls), maria, and pyroclastic deposits. Fig. 2 shows an example observation of the Reiner Gamma swirl with incidence angle ~ 63°, emission angle ~ 83°, and phase angle ~ 147°. The signal measured by the LR telescope

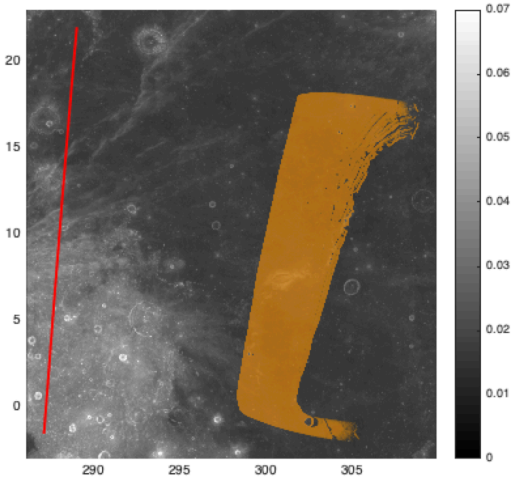

Figure 2 - Map view of an observation of Reiner Gamma with the sub-LRO ground track (red) and LOLA-LR FOV (orange).

in Fig. 3 is expressed as the radiance factor (RADF), the ratio of the measured radiance to that of a perfectly diffuse Lambert sphere illuminated vertically. We compute an initial model RADF (Fig. 3) by performing a 3-D ray-tracing with the 64 pix/° LOLA shape model using our IllumNG illumination code [9]. The FOV is sampled with 500 sightlines and, for each one, we determine its intersection point on the shape model and whether or not that point can see the Sun and LRO. The predicted radiance from each unobscured sightline is calculated by interpolating the spatially-resolved multi-wavelength LRO Wide Angle Camera (WAC) Hapke parameter maps [8] in lon/lat and wavelength. Thus, it uses Hapke parameters appropriate for the actual surface locations in the FOV at ~532-nm. Note that variations in the parameters on scales smaller than the map resolution of 1° will not be completely captured by the interpolation, but given the large FOV and oblique viewing geometry, it is unlikely we could resolve smaller variations in the longitudinal (cross-track) direction. Latitudinal (along-track) variations are more easily resolved due to the high sampling rate. The offset between the data and initial model is unlikely to be due to the LR radiometric zero-point since multiple observations of other locations at phase < 90° show good agreement (within ~10%) between the data and initial model.

We compute the best fit to the LOLA-LR data (Fig. 3) by varying one free parameter from its initial value in many 1°-square bins shown in Fig. 4. Here, we consider two alternative end-member Hapke models: varying the photometric surface roughness θ or the 2-term Henyey-Greenstein (HG) asymmetry parameter, *c*. In the Hapke model, the surface roughness is parameterized by θ, the mean surface slope on photometrically relevant size scales [2]. Evidence suggests that, at visible wavelengths, these scales are on the order of 0.1 mm to 0.1 cm [10,11]. The HG asymmetry parameter controls the relative strength of forward vs. backward scattering in the single particle phase function [2] and varies in the range [-1, 1] where values < or > 0 indicate the phase function is mostly forward- or backward-scattering, respectively. In the WAC Hapke maps, the initial value of θ is constant at 23.4° and the initial values of *c* range from ~ 0.0 to 0.1 [8].

Adjusting θ or *c* from their initial values results in a nearly identical final best fit model, thus, only one is shown in Fig. 3. However, variations in *c* significantly degrade the model's agreement with the WAC data at lower phase (Fig. 4). These preliminary results suggest that the LOLA-LR data are most easily explained by variations in roughness and that Reiner Gamma is smoother than the surrounding maria on sub-mm to sub-cm scales. However, it is possible that multiple parameters are varying simultaneously from their initial values. Therefore, future work will investigate co-adjusting multiple parameters, as well as using a higher-resolution shape model and albedo map. As LRO's extended science mission continues, we will conduct more such high-phase observations to study the effects of space weathering and geologic history on regolith surface photometric properties.

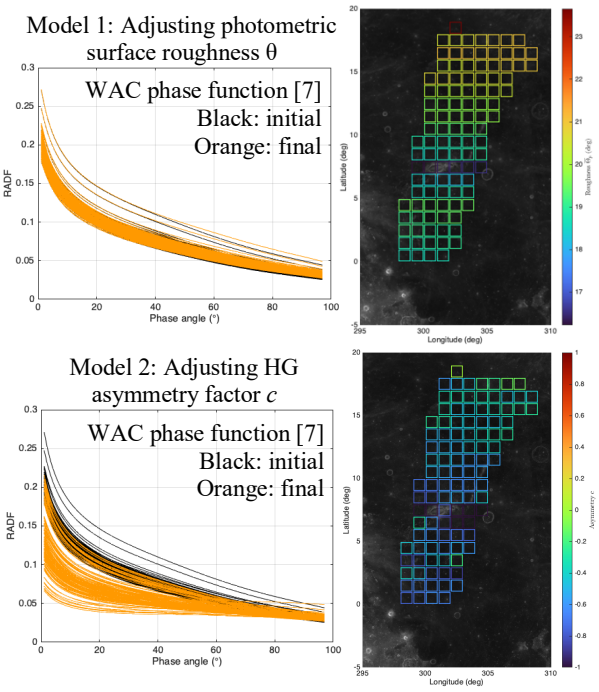

Figure 4 – Final best fit models adjusting photometric surface roughness, θ, and HG asymmetry factor, *c*.

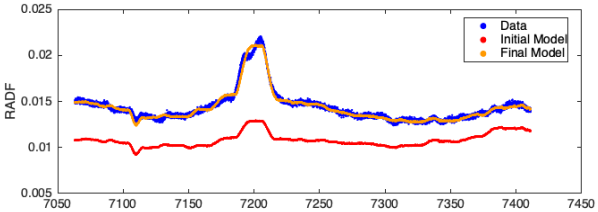

Figure 3 - Measured signal (blue) compared with initial (red) and final best fit (orange) model.

References: [1] Joliff, B. et al., Eds. (2006) Berlin: De Gruyter, "New Views of the Moon", *Rev. in Mineralogy & Geochem.*, 60. [2] Hapke, B. (2012) Camb. Univ. Press, *Theory of Refl. and Emitt. Spectr.*, 2nd ed. [3] Labarre, S. et al. (2017) *Icarus*, 290, 63. [4] Zuber M. T. et al. (2010) *Space Sci. Rev.,* 150, 63. [5] Barker, M. K. et al. (2016) *Icarus*, 273, 96. [6] Karpenko, M. et al. (2020) AAS/AIAA Astrodyn. Spec. Conf., AAS 20-574. [7] Denevi, B. W et al. (2016) *Icarus*, 273, 53. [8] Sato, H. et al. (2014) *JGR Planets,* 119, 1775. [9] Mazarico, E. et al. (2018) *Adv. in Space Res.*, 62, 3214. [10] Cord, A. M. et al. (2003) *Icarus*, 165, 414. [11] Helfenstein, P. & Shepard, M. K. (1999) *Icarus*, 141, 107.